Journal of Medicinal Chemistry Article

J. Med. Chem. **2009,** *52,* 4257–4265 **4257**
DOI: 10.1021/jm900411s

A Small-Molecule Inhibitor of Nipah Virus Envelope Protein-Mediated Membrane Fusion

Sabine Niedermeier,[†,⊥] Katrin Singethan,[‡,⊥] Sebastian G. Rohrer,[§] Magnus Matz,[§] Markus Kossner,[§] Sandra Diederich,[∥] Andrea Maisner,[∥] Jens Schmitz,[†] Georg Hiltensperger,[†] Knut Baumann,[§] Ulrike Holzgrabe,*[,†] and Jurgen Schneider-Schaulies*[,‡]

[†]*Institute of Pharmacy and Food Chemistry, University of Wurzburg, Am Hubland, 97080 Wurzburg, Germany,* [‡]*Institute for Virology and Immunobiology, University of Wurzburg, Versbacher Strasse 7, 97078 Wurzburg, Germany,* [§]*Institute for Pharmaceutical Chemistry, Technical University of Braunschweig, Beethovenstrasse 55, 38106 Braunschweig, Germany, and* [∥]*Institute for Virology, University of Marburg, Hans-Meerweinstrasse 2, 35043 Marburg, Germany.* [⊥]*Both authors contributed equally to this work.*

Received December 16, 2008

Nipah virus (NiV), a highly pathogenic paramyxovirus, causes respiratory disease in pigs and severe febrile encephalitis in humans with high mortality rates. On the basis of the structural similarity of viral fusion (F) proteins within the family *Paramyxoviridae*, we designed and tested 18 quinolone derivatives in a NiV and measles virus (MV) envelope protein-based fusion assay beside evaluation of cytotoxicity. We found five compounds successfully inhibiting NiV envelope protein-induced cell fusion. The most active molecules (**19** and **20**), which also inhibit the syncytium formation induced by infectious NiV and show a low cytotoxicity in Vero cells, represent a promising lead quinolone-type compound structure. Molecular modeling indicated that compound **19** fits well into a particular protein cavity present on the NiV F protein that is important for the fusion process.

Introduction

Zoonotic outbreaks of respiratory disease and encephalitis affecting humans, horses, and pigs in Australia, Malaysia, and Singapore have led to the isolation of two novel paramyxoviruses, i.e., Hendra and Nipah virus, which have been assigned to the new genus Henipavirus in the family *Paramyxoviridae*.[1−3] The natural host of NiV are fruit bats of the genus *Pteropus*.[4,5] In September 1998, NiV[a] emerged in Malaysia and Singapore first in pigs and then in humans, mainly pig farmers.[6] While causing respiratory disease and encephalitis with low mortality rates in pigs, a severe febrile encephalitis with high mortality rates was observed in NiV-infected humans (case fatality rate approximately 40%). Further spread of virus could be controlled by killing over a million pigs. By the end of December 1999, a total of 276 human cases of acute encephalitis including 106 deaths were recorded. More recent outbreaks of NiV infections in Bangladesh and India have led to further human deaths and may have been a result of both direct bat-to-human and human-to-human transmissions.[7−10]

Endothelial cells are the major cellular targets for NiV, and syncytia of endothelial cells in blood vessels are recognized as characteristic feature of the NiV infection.[11] In concordance with the viral tropism, the transmembrane proteins EphrinB2 and EphrinB3, expressed on endothelial cells, neurons, and the smooth muscle cells surrounding arterioles, were identified as cellular entry receptors for NiV.[12,13] Virus uptake into target cells is mediated by the viral envelope glycoproteins G (attachment) and F (fusion). After cleavage of the precursor F protein in F_1 and F_2 subunits, they form an active $G/F_{1/2}$ complex mediating pH independent virus−cell and cell−cell fusion.[14−16] The fact that the fusion proteins of *Paramyxoviridae* share several features with other viral glycoproteins responsible for membrane fusion, including the hemagglutinin (HA) of influenza virus, gp41 of human immunodeficiency virus, gp of Ebola virus, and the F proteins of respiratory syncytial virus (RSV) and simian virus 5 (SV5), may facilitate further structural analyses.[17−19] The crystal structure of the Nipah and Hendra virus core F proteins,[20,21] and the NiV G attachment protein were elucidated recently.[22,23]

Small molecule inhibitors fitting into a pocket of the measles virus (MV) F protein, another member of the *Paramyxoviridae*, and preventing membrane fusion have been designed earlier.[24−26] Given the structural similarity of the paramyxoviral F proteins, we tested some of these small molecule inhibitors and a library of quinolone derivatives in a NiV F protein-based fusion assay. We found that certain compounds, different from the most active molecules against measles, successfully inhibited NiV envelope protein-induced cell fusion. Computer modeling suggested that they fit well into a protein cavity present in the NiV F protein.

Chemistry

The quinolone skeletons were built up using the Gould−Jacobs procedure starting with the correspondingly substituted aniline derivatives **1**.[27] In analogy to Leyva et al.,[28] condensation with diethyl ethoxymethylene malonate and

*To whom correspondence should be addressed. For U.H., medicinal chemistry: phone, ++49 931-888-5460, fax, ++49 931-888-5494; E-mail, u.holzgrabe@pharmazie.uni-wuerzburg.de. For J.S.-S., virology: phone, ++49 931-201-49895; fax, ++49 931-201-49553; E-mail: jss@vim.uni-wuerzburg.de.

[a]Abbreviations: DAPI, 4′,6-diamidino-2-phenylindole; EGFP, enhanced green fluorescent protein; ELISA, enzyme-linked immunosorbent assay; FCS, fetal calf serum; F glycoprotein, fusion glycoprotein; G glycoprotein, attachment glycoprotein; gp, glycoprotein; HA, hemagglutinin; HR, heptad repeat; MDCK, Madin−Darby canine kidney; MEM, minimal essential medium; MOI, multiplicity of infection; MTT, 3-(4,5-dimethylthiazol-2-yl)-2,5-diphenyl-tetrazoliumbromide; MV, measles virus; NiV, Nipah virus; PDB, Protein Data Bank; PEI, polyethylenimine; PyBOB, benzotriazol-1-yl-oxy-tris-pyrrolidino-phosphonium hexafluorophosphate; rmsd, root-mean-square deviation; rt, room temperature.

Published on Web 06/05/2009

Scheme 1. Synthesis Pathway[a]

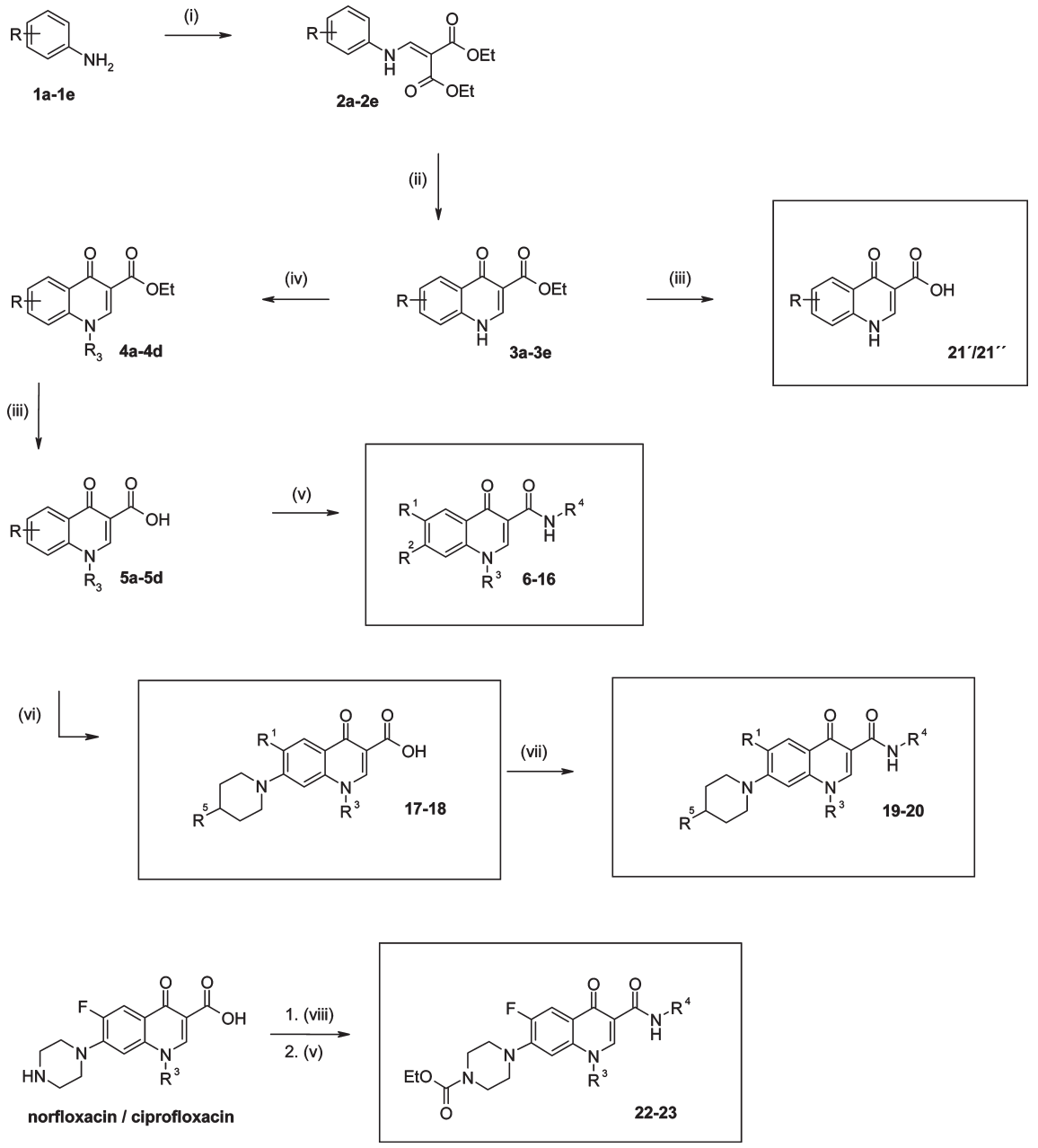

[a] Reagents: (i) diethyl ethoxymethylene malonate, toluene, reflux; (ii) diphenyl ether, reflux; (iii) EtI, NaOH, DMSO, rt; (iv) NaOH, EtOH, 90 °C, HCl; (v) $ClCO_2Et$, NEt_3, DMF, 0 °C; H_2N-R_4, 0 °C/rt; (vi) piperidine derivative, DMF; (vii) PyBOB, H_2N-R_4, DMF; (viii) $ClCO_2Et$, NEt_3, DMF, 0 °C/rt.

Scheme 2. Structural formulae of compounds **24**, **25**, and **26**

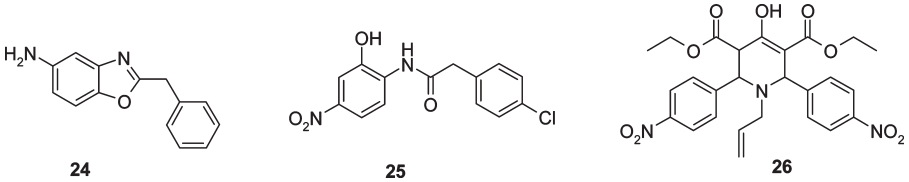

subsequent thermal cyclization in diphenyl ether revealed the 4-quinolone-3-carboxylic esters **3a**−**3e**. In some cases, a mixture of regioisomers, substituted in the 5- or 7-position, was obtained. A separation of these isomers using column chromatography was performed on the esters **4c** and **4d**. *N*-Alkylation of **3a**−**3e** with ethyl iodide in presence of NaOH/DMSO led to the ethyl 1-ethyl-4-quinolone-3-carboxylates **4a**−**4d**.[29] Ester hydrolysis of **4** achieved the quinolone-3-carboxylic acids **5a**−**5d**, which can be coupled with an appropriate amine applying the method of mixed anhydrides with ethyl chloroformate to give the 4-*oxo*-1,4-dihydroquinoline-3-carboxamides **6**−**16**.[30] Substitution of the chloro atom

in position 7 of 7-chloro-1-cyclopropyl-6-fluoro-4-*oxo*-1,4-dihydroquinoline-3-carboxylic acid and 7-chloro-1-ethyl-6-fluoro-4-*oxo*-1,4-dihydroquinoline-3-carboxylic acid, respectively, with corresponding piperidine derivatives resulted in compounds **17** and **18**. By means of benzotriazol-1-yl-oxy-tris-pyrrolidino-phosphonium hexafluorophosphate (PyBOB) as activating agent, conversion of **17** and **18** with 2,4-dichlorobenzylamine gave the corresponding 7-substituted 4-quinolone-3-carboxamides **19** and **20**, respectively.[31] However, some of the compounds **2**, **3**, **4**, and **5** are already described in the literature (see Supporting Information).[32−36]

Regioisomeric mixtures of the dicarboxylates **21′/21″**, substituted in 5- or 7-positon, were obtained via concomitant hydrolysis of the ester and the nitrile function of **3e′** and **3e″**, respectively. The ratios of these isomers were determined by NMR spectroscopy monitoring the signal of the proton in position 2. It was not possible to completely separate the isomers **21′/21″** (see Scheme 1).

To evaluate the relevance of the piperidine ring, piperazine derivatives, analogous to compound **19** and **20**, were synthesized by converting the basic piperazine nitrogen of norfloxacin and ciprofloxacin, respectively, with ethyl chloroformate to achieve the corresponding carbamates, and by amidation of the carboxylate function in position 3 with 2,4-dichlorobenzylamine to eventually yield compounds **22** and **23**.

Results and Discussion

On the basis of the structural similarity of the *Paramyxoviridae* F proteins, the two measle fusion inhibitors 2-benzyl-benzooxazol-5-yl-ammonium chloride **24** (**OX-1**) and

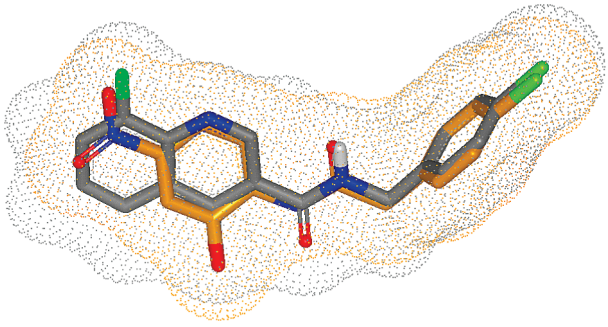

Figure 1. Compound **25** (orange carbons, orange surface) aligned to *N*-(4-chlorobenzyl)-8-fluoro-4-*oxo*-1,4-dihydroquinoline-3-carboxamide (gray carbons, blue surface), which was ranking top on the ROCS hitlist.

Table 1. Substitution Pattern of All Quinolone Derivatives Synthesized

compd.	R^1 / R^2	R^3	R^4	compd.	R^1 / R^2 / R^5	R^3	R^4
6	R^1 = F	Et	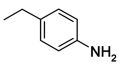	**15**	R^2= CF_3	Et	
7	R^1 = CF_3	Et	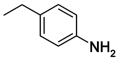	**16**	R^2 = CF_3	Et	
8	R^1 = F	Et		**17**	R^1 = F, R^5 = 		-
9	R^1= CF_3	Et		**18**	R^1 = F, R^5 = 	Et	-
10	R^1 = F	Et		**19**	R^1 = F, R^5 = 		
11	R^2 = CF_3	Et		**20**	R^1 = F, R^5 = 	Et	
12	R^2 = CF_3	Et	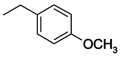	**21′/21″**	R = COOH	-	-
13	R^1 = F, R^2 = Cl	Et	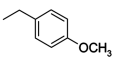	**22**	-	Et	
14	R^2 = CF_3	Et	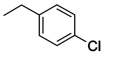	**23**	-		

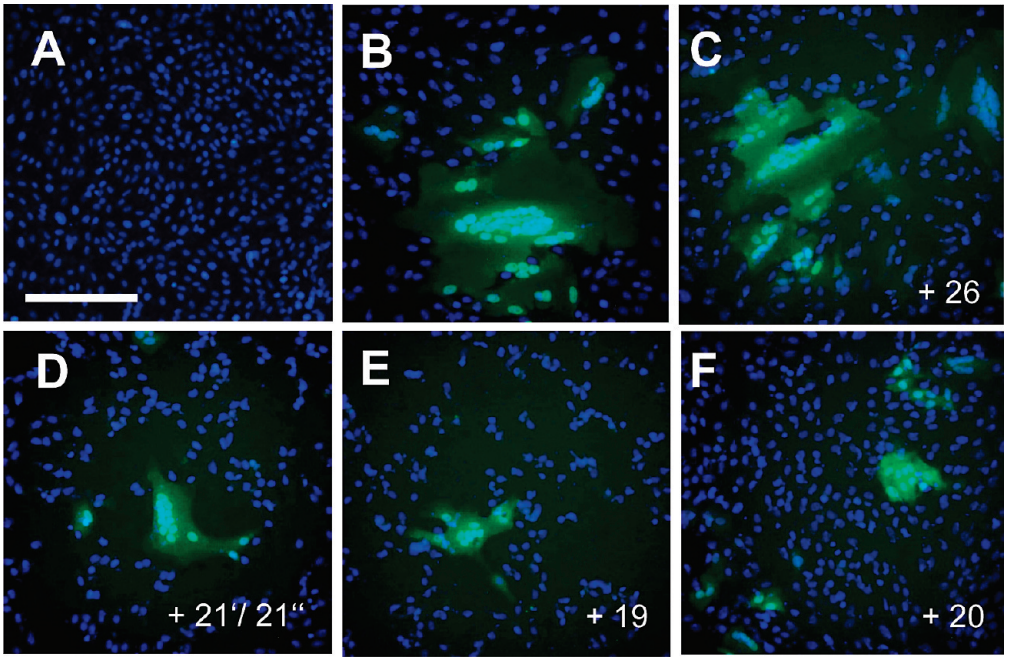

Figure 2. Syncytium formation in the absence and presence of inhibitors. Vero cells were transfected with expression vectors for the NiV G and F proteins and the enhanced green fluorescent protein (EGFP). Inhibitors were added after transfection at 4 μM, and the cells incubated for 24 h at 37 °C. After fixation and permeabilization of the cells, nuclei were stained with DAPI (blue). (A) Untransfected control cells (bar = 100 μm). (B) Transfected cells in the absence of inhibitors showing a large and several smaller syncytia; (C−F) cells in the presence of 4 μM **21′/21″** (1:2), **19**, **20**, and **26**, respectively, as indicated.

2-(4-chorophenyl)-*N*-(2-hydroxy-4-nitrophenyl)acetamide **25** (**AM-2**)[24] were utilized as template substances for virtually screening the MDL Drug Data Report (Scheme 2).[37] Three-dimensional similarity searching was carried out using the program OpenEye ROCS,[38] which is based on a Gaussian representation of the molecular surfaces for the rapid overlay of molecules. Molecular similarity was quantified by the ROCS "combo score", a metric considering both molecular shape and pharmacophore-based similarity. A frequently retrieved scaffold from the virtual screen was 1,4-dihydroquinolone-3-carboxylic acid (compare to **5a**−**5d** and **21′/21″**, Scheme 1). One of the top scoring molecules exhibiting this scaffold aligned with **25** is shown in Figure 1. This scaffold was consequently used as the core to design a library of compounds to be tested in fusion inhibition assays (Table 1). However, the 1,4-dihydroquinolone-3-carboxylic acid derivatives are well-known as antibacterial agents and are therefore widely used in the treatment of infections.[39,40]

To induce virus−cell or cell−cell fusion, both viral envelope proteins, G (interacting with the cellular receptor) and F (inserting the hydrophobic fusion peptide into the target cell membrane), are required. To determine the capacity of the small molecules to inhibit viral envelope protein-mediated membrane fusion, we transfected Vero cells with expression vectors for NiV G and F[15] and quantified the formation of syncytia. Twenty-four h after transfection, control cells showed extensive syncytium formation containing syncytia with up to 30 nuclei. After addition of inhibitors, the size of the syncytia (average number of nuclei in syncytia) was determined in the microscope. Examples of the effect of the compounds on syncytium formation in tissue culture with the noninhibitory substance diethyl (2*R*,6*S*)-1-allyl-4-hydroxy-2,6-bis(4-nitrophenyl)-1,2,3,6-tetrahydropyridine-3,5-dicarboxylate (**26**)[41] and three inhibitory substances (**21′/21″** (1:2), **19**, and **20**) are shown in Figure 2.

To quantify the inhibitory effect of the substances in a dose-dependent manner, the average number of nuclei in syncytia of control cells was set to 100% and the number of nuclei in syncytia in the presence of inhibitors is presented in relation to the untreated control in Figure 3A. The inhibitory activity of the most potent compounds is summarized in Table 2. In concentrations between 10 and 200 μM all other compounds were found to be inactive or cytotoxic (data not shown). Among the inhibitors, compound **19** was the most effective NiV-fusion inhibitor followed by **20**, **22**, and **23**, and with some restrictions due to the isomeric mixture **21′/21″** (1:2), with EC_{50} values of approximately 1.5, 4, 3, and 8 μM, respectively. The substance **24**[26] used as reference in this experiment was not active against NiV-induced cell fusion. In comparison, we also determined the inhibitory capacity of these compounds in a MV H/F-fusion assay (Figure 3B). Here we found that benzoxazole **24** was the most active inhibitor, followed by **14**, **20**, and **21′/21″** (1:2), whereas **19** was less active. In both cases, NiV and MV-induced cell fusion, compound **26** was inactive.

Comparing the *N*-benzylamides **19**/**20** and **22**/**23** the following structure−activity relationships can be derived: Whereas varying substitution of the quinolone nitrogen (N1), i.e., ethyl and cyclopropyl, does not alter the activity (cf. compound **22** and **23**) for both MV and NiV, the substituted piperidine and piperazine rings at position 7 have a different influence on the fusion inhibition of NiV and MV, indicating structural difference in the binding site. While the carbamoylated piperidine and piperazine substituted compounds **20**, **22**, and **23** show almost the same anti-NiV EC_{50} values (3−4 μM), the anti-MV EC_{50}s differ by a factor of 7 (cf. **22**/**23** and **20**). However, the highest anti-NiV and anti-MV activity resides on the piperidine derivatives. On the basis of the series of compounds studied here, it is difficult to explain the similar anti-MV activity of the structurally heterogeneous compounds **14**, **20**, and **21**.

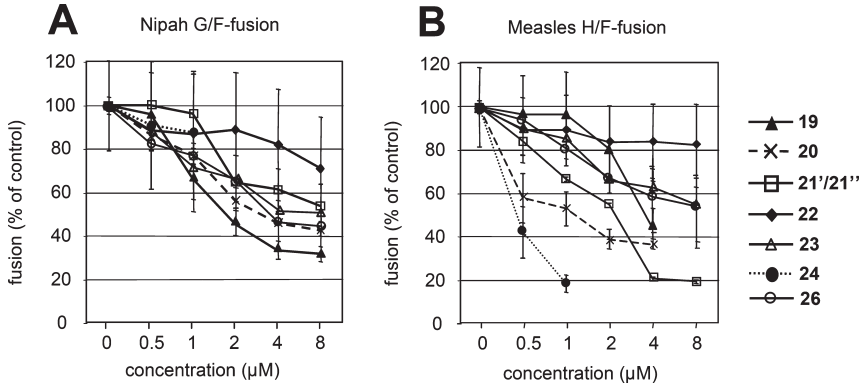

Figure 3. Dose-dependent inhibition of cell fusion. Vero cells were transfected with plasmids expressing the NiV G and F proteins (A) or the MV HA and F proteins (B). Inhibitors were added after transfection in concentrations as indicated and the cells incubated for 24 h at 37 °C. Average numbers of nuclei in at least 50 syncytia per concentration per compound were quantified using the microscope. Relative fusion is presented as percentage in relation to the untreated control cells (100%). $N = 3$ independent experiments, standard deviations are given.

Table 2. Cell−Cell Fusion Inhibiting Activity Determined in NiV-G/F and MV-H/F-Transfected Vero Cells and Cytotoxicity of Selected Compounds

compd	anti-NiV EC_{50} (μM)	anti-MV EC_{50} (μM)	CC_{50} (μM)[a]	SI (CC_{50}/EC_{50})
24	> 8	0.4	8	20 (MV)
14	> 8	2	> 20	> 10 (MV)
15	(toxic)	(toxic)	> 20	
19	1.5	4	> 20	> 13 (NiV)
20	3	1.5	10	3.3 (NiV)
21′/21″ (1:2)	8	2.5	> 20	
22	4	10	> 20	3.75 (NiV)
23	3	10	15	5.0 (NiV)
26	> 20	> 20	> 20	

[a] The cytotoxicity (CC_{50}) was determined using the MTT test (materials and methods) and nontransfected Vero cells.

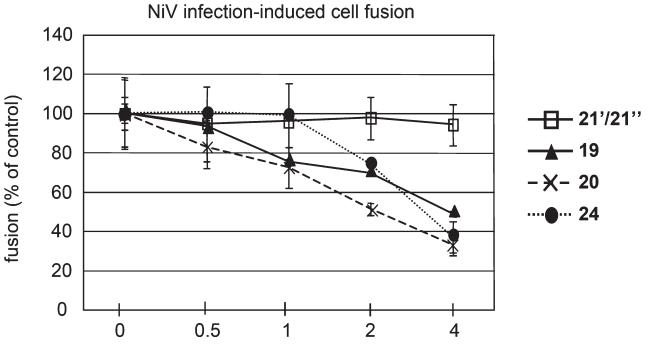

Figure 4. Inhibition of virus-mediated cell fusion. Vero cells were infected with NiV at an MOI of 0.2 in the presence of various concentrations of the compounds **21′/21″**(1:2), **19**, **20**, and **24**, incubated for 24 h at 37 °C, fixed with 4% paraformaldehyde for 48 h, and stained with a guinea pig antiserum directed against NiV and DAPI to facilitate counting of nuclei. The number of nuclei in syncytia of inhibitor-treated cells were counted and are presented as percentages of the number of nuclei in syncytia of cells without inhibitors (100%).

The cytotoxicity of the compounds for Vero cells was determined in a cell vitality assay demonstrating variable toxicities of the compounds investigated. CC_{50} results are included in Table 2. Interestingly, the most active inhibitor of the NiV cell fusion, compound **19**, shows the lowest cytotoxicity, resulting in an SI value of >13.

To confirm the fusion-inhibitory activity determined after transfection of the envelope proteins in an infection-inhibition assay with infectious NiV, we infected Vero cells with NiV at a multiplicity of infection (MOI) of 0.2 for 24 h in the absence and presence of **21′/21″** (1:2), **19**, **20**, and **24**. All work with live virus was performed under biosafety level-4 conditions. In concentrations of 0.5 to 4 μM, the NiV infection-induced syncytium formation was dose dependently reduced by **19**, **20**, and **24**, but not by **21′/21″** (1:2), which prompted us to stop the isomer separation attempts (Figure 4). Thus, syncytium formation was not only successfully inhibited after transfection of envelope proteins expressing plasmids but also after infection of cells with live NiV with compounds **19** and **20**.

The crystal structure of the NiV postfusion coiled coil trimer (PDB: 1WP7[20]) was published while the synthesis work was done and can thus be used to retrospectively suggest a binding mode for the biologically active compounds by computer modeling. Analyzing the interface between heptad repeats 1 and 2 (HR1−HR2 interface), which is deemed essential for HR1−HR2 binding, and thus for NiV fusion, reveals that the hydrophobic interactions between I474, L481, and V484 in HR2 and the corresponding hydrophobic pockets in HR1 (Figure 5) are of utmost importance. This is in accord with a previously published study.[42] Thus, the corresponding region in HR1 (deep groove, Figure 5A) was used as the binding pocket for the subsequent docking steps.

Figure 5B shows the highest scoring pose of inhibitor **19**. It is obvious, that **19** can interact favorably with the HR-1 major groove binding pocket. Particularly, the fluoro-substituted phenyl residue replaces I474 in the large hydrophobic binding site, the cyclopropyl residue constitutes a bioisosteric replacement for L481, and the piperidine effectively replaces V484. In addition, **19** exhibits only moderate solvent exposure. In comparison, Figure 5C shows the highest scoring pose of inhibitor **15**, which also fits into the binding pocket, but owing to its smaller size and altered geometry cannot address the hydrophobic binding pockets as well as **19**. Hence, the docking score of compound **15** is inferior, which actually corresponds here to the lower bioactivity that was measured for this compound. The inability to interact with the hydrophobic pocket holds true for all less and inactive compounds because they all miss a saturated heterocycle in position 7.

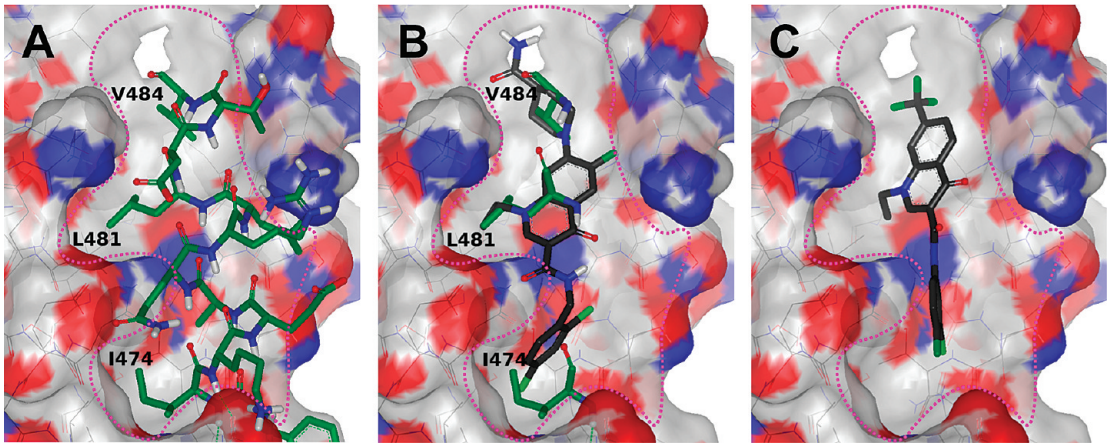

Figure 5. (A) Essential hydrophobic interactions between HR2 (green) and HR1 (surface). The binding of the HR2 amino acids I474, L481, and V484 into hydrophobic sites in the binding pocket of HR1 (pink dashes) is required for NiV fusion. (B) Structural overlay of the predicted binding mode of inhibitor **19** and the binding mode of HR2 in the NiV F-protein crystal structure (PDB 1WP7). The side chains of inhibitor **19** provide bioisosteric replacements of the HR2 amino acids (green) essential for HR1−HR2 binding. (C) Predicted binding mode of inhibitor **15**. Because of the tight binding of the trifluormethyl residue to the upper hydrophobic site (V484), the lower hydrophobic site (I474) cannot be addressed.

Conclusion

The comparison of NiV with the related MV-based cell fusion experiments revealed that the reference compound **24**[26] is MV specific, whereas compounds **19**, **22**, and **23** are NiV specific and **21′**/**21″** (1:2) and **20** inhibit both viruses with an intermediate efficiency. The EC_{50} values and CC_{50}/EC_{50} ratios presented in Table 2 are based on the inhibition of cell−cell fusion after transfection of Vero cells with NiV G and F, or MV H and F as described above and not as usual on infection-inhibition assays with complete virus and therefore may not exactly reflect the natural situation. However, the results were confirmed by data obtained with infectious NiV, demonstrating that the inhibitory activity of the compounds was also present in the context of complete infectious viruses. In conclusion, this study revealed a class of promising compounds that fit into a particular protein cavity of the NiV F protein, inhibit NiV-induced virus-cell and cell−cell fusion, and show relatively low cytotoxicity.

Experimental Section

Melting points were determined with a Stuart melting point apparatus SMP11 (Bibby Scientific, UK) and not corrected. IR spectra were obtained using a Biorad PharmalyzIR FT-IR spectrometer (Digilab, Krefeld, Germany). TLC was performed on silica gel 60 F_{254} aluminum sheets (Merck, Darmstadt, Germany). ^{1}H (400.132 MHz) and ^{13}C (100.613 MHz) NMR spectra were recorded on a Bruker AV 400 instrument (Bruker Biospin, Ettlingen, Germany). Abbrevations for data quoted are: s, singlet; d, doublet; t, triplet; q, quartet; m, multiplet; b, broad; dd, doublet of doublets; dt, doublet of triplets. The center of the peaks of $CDCl_3$ (^{1}H: 7.26 ppm; ^{13}C: 77.16 ppm) and DMSO-d_6 (^{1}H: 2.50 ppm; ^{13}C: 39.52 ppm) were used as internal references. Coupling constants (J) are given in Hz. Chemicals were of analytical grade and purchased from Aldrich (Steinheim, Germany) and Merck (Darmstadt, Germany). Some of the compounds **2**, **3**, **4**, and **5** are already described in the literature (see Supporting Information). However, a general synthesis procedure is given in the Supporting Information. Microanalyses (C, H, N) of the new compounds agreed with the theoretical value within ±0.4%.

Synthesis of *N*-(Cyclopropylmethyl)-1-ethyl-6-fluoro-4-*oxo*-1,4- *N*-(4-Chlorobenzyl)-1-ethyl-4-*oxo*-7-(trifluoromethyl)-1, 4-dihydroquinoline-3-carboxamide (14). Compound **5c** (1 equiv, 2 mmol) and 2.1 equiv (4.2 mmol) of triethylamine were dissolved in abs DMF (20 mL). Ethyl chloroformate (2.05 equiv, 4.1 mmol) were added under stirring at 0 °C for 1.5 h. After addition of 1.2 equiv (2.4 mmol) of 4-chlorobenzylamine, the reaction mixture was stirred at 0 °C for 1 h and subsequently at room temperature for 72 h. The precipitate was filtered and recrystallized from a mixture of water and ethanol (9:1) to give **14**. Yield 31%; mp 195−197 °C. IR [cm^{-1}]: 802, 878, 955, 1076, 1160, 1312, 1443, 1534, 1602, 1665, 2979, 3049, 3222. ^{1}H NMR (DMSO-d_6, δ [ppm], J [Hz]): 1.39 (t, J = 7.1, CH_3), 4.64−4.61 (m, 2 × CH_2), 7.35−7.31 (m, 2 × benzyl-H), 7.49−7.40 (m, 2 × benzyl-H), 7.85 (d, J = 8.4, H-6), 8.24 (s, H-8), 8.55 (d, J = 8.4, H-5), 9.00 (s, H-2), 10.27 (t, J = 5.9, NH). ^{13}C NMR (DMSO-d_6, δ [ppm], J [Hz]): 14.4 (CH_3), 40.3 (CH_2), 48.5 (CH_2), 55.0 (CH_3), 111.8 (C-3), 115.2 (q, $J_{C,F}$ = 4.1, C-8), 120.8 (q, $J_{C,F}$ = 3.3, C-6), 123.6 (q, J = 273.5, CF_3), 127.3 (benzyl-C), 128.2 (C-5), 128.8 (benzyl-C), 129.2 (benzyl-C), 129.3 (benzyl-C), 129.6 (C-4a), 132.3 (benzyl-C), 132.6 (q, $J_{C,F}$ = 32.7, C-7), 136.3 (benzyl-C), 138.6 (C-8a), 149.2 (C-2), 163.8 (C-9), 174.7 (C-4).

General Procedure for the Synthesis of 7-(4-Carbamoylpiperidin-1-yl)-1-cyclopropyl-*N*-(2,4-dichlorobenzyl)-6-fluoro-4-*oxo*-1,4-dihydroquinoline-3-carboxamide (19) and Ethyl 1-[3-(2, 4-Dichlorobenzylcarbamoyl)-1-ethyl-6-fluoro-4-*oxo*-1,4-dihydroquinoline-7-yl]piperidine-4-carboxylate (20). Compounds **17** and **18** (1 equiv, 1.1 mmol), 1.1 equiv (1.2 mmol) of benzotriazol-1-yl-oxy-tris-pyrrolidino-phosphonium hexafluorophosphat (PyBOB) and 3 equiv (3.2 mmol) of 2,4-dichlorbenzylamine were dissolved in abs DMF (20 mL). The mixture was stirred at room temperature for 24 h and subsequently at 120 °C for 6 h. After removing the solvent in vacuo, the residue was purified by column chromatography on silica gel (eluent: ethyl acetate/ethanol 7:3) to give **19** and **20**, respectively. **19**: yield 33%; mp 180 °C. IR [cm^{-1}]: 829, 1031, 1251, 1476, 1531, 1666, 2928, 3089, 3241. ^{1}H NMR (DMSO-d_6, δ [ppm], J [Hz]): 1.16 (b, 2 × cyclopropyl-H), 1.29−1.32 (m, 2 × cyclopropyl-H), 2.00−2.08 (m, 4 ×, piperinyl-H), 2.39−2.44 (m, piperinyl-H), 2.90−2.98 (m, 2 × piperinyl-H), 3.45 (b, cyclopropyl-H), 3.73−3.76 (m, 2 × piperinyl-H), 4.68 (d, J = 6.0, CH_2), 5.57/5.46 (2 × s, $CONH_2$), 7.19 (dd, J = 8.2, J = 2.1, benzyl-H), 7.24 (d, J = 8.2, benzyl-H), 7.31 (d, $J_{F,H}$ = 7.3, H-8), 7.37 (d, J = 2.1, benzyl-H), 8.01 (d, $J_{F,H}$ = 13.2, H-5), 8.80 (s, H-2), 10.49 (t, J = 6.0, NH). ^{13}C NMR (DMSO-d_6, δ [ppm], J [Hz]): 8.0 (2 × cyclopropyl-C), 28.5 (2 × piperinyl-C), 34.6 (2 × cyclopropyl-C), 40.4 (CH_2), 41.8 (piperinyl-C), 49.6 (2 × piperinyl-C), 104.7 (d, $J_{F,C}$ = 2.9, C-8), 110.8 (C-3), 112.5 (d, $J_{C,F}$ = 23.4, C-5), 121.5 (d, $J_{C,F}$ = 6.7, C-4a), 126.9 (benzyl-C), 129.0 (benzyl-C), 130.2 (benzyl-C), 133.3 (benzyl-C), 134.0 (benzyl-C), 134.8 (benzyl-C), 138.3 (C-8a),

145.0 (d, $J_{C,F}$ = 10.2, C-7), 146.6 (C-2), 153.3 (d, $J_{C,F}$ = 249.5, C-6), 165.1 (CONH), 175.3 (d, $J_{C,F}$ = 2.2, C-4), 175.3 ($CONH_2$). **20**: yield 38%; mp 217−218 °C. IR [cm^{-1}]: 826, 1039, 1171, 1309, 1489, 1530, 1664, 1737, 2985, 3258. ^{1}H NMR (DMSO-d_6, δ [ppm], J [Hz]): 1.28 (t, J = 7.1, CH_3), 1.54 (t, J = 7.2, CH_3), 1.94−2.03 (m, 2 × piperinyl-H), 2.07−2.11 (m, 2 × piperinyl-H), 2.50−2.59 (m, piperinyl-H), 2.92−2.99 (m, 2 × piperinyl-H), 3.61−3.64 (m, 2 × piperinyl-H), 4.18 (d, J = 7.1, CH_2), 4.23 (q, J = 7.2, CH_2), 4.70 (d, J = 6.0, CH_2), 6.80 (d, J = 8.3, benzyl-H), 7.19 (dd, J = 8.3, J = 2.0, benzyl-H), 7.38 (d, J = 2.0, benzyl-H), 7.40 (d, $J_{F,H}$ = 8.6, H-8), 8.08 (d, $J_{F,H}$ = 13.1, H-5), 8.70 (H-2), 10.54 (t, J = 6.0, NH). ^{13}C NMR (DMSO-d_6, δ [ppm], J [Hz]): 14.4 (CH_3), 14.6 (CH_2), 28.1 (2 × piperinyl-C), 40.7 (piperinyl-C), 49.3 (CH_2), 49.9 (2 × piperinyl-C), 60.8 (CH_2), 104.0 (d, $J_{C,F}$ = 2.2, C-8), 111.4 (C-3), 113.2 (d, $J_{C,F}$ = 22.7, C-5), 122.6 (d, $J_{C,F}$ = 6.7, C-4a), 127.3 (benzyl-C), 129.3 (benzyl-C), 130.5 (benzyl-C), 133.5 (benzyl-C), 134.3 (benzyl-C), 135.2 (benzyl-C), 136.7 (C-8a), 145.6 (d, $J_{C,F}$ = 11.0, C-7), 146.8 (C-2), 153.5 (d, $J_{C,F}$ = 249.6, C-6), 165.5 (C-4), 174.5 (CO_2Et), 175.5 (d, $J_{C,F}$ = 2.2, C-4).

General Procedure for the Synthesis of 4-*oxo*-1,4-Dihydroquinoline-3,5-dicarboxylic Acid (21′) and 4-*oxo*-1,4-Dihydroquinoline-3,7-dicarboxylic Acid (21″). Compounds **3e′**/**3e″** (10 mmol) were dissolved in an aqueous sodium hydroxide solution (10%) and heated at 90 °C for 50 min. The mixture was cooled to room temperature, and aqueous conc hydrochloride acid solution added until pH = 2. The precipitate was filtered, washed several times with water, and dried in vacuo to give **21′**/**21″**, a mixture of regioisomers substituted in the 5- or 7-position. The ratio of the isomers was determined by NMR spectroscopy. **21′**/**21″**(1:2): yield 97%; mp > 350 °C. IR [cm^{-1}]: 809, 907, 1069, 1202, 1385, 1594, 1634, 1645, 1698, 2993, 3063, 3217. ^{1}H NMR (DMSO-d_6, δ [ppm], J [Hz]): **21′**: 8.00 (t, J = 7.6, H-7), 8.08 (d, J = 7.6, H-6), 8.88 (s, H-2), 8.18−8.21 (m, H-8), 14.16 (b, NH), 15.05 (b, COOH). **21″**: 8.01 (dd, J = 8.6, J = 1.7, H-6), 8.35 (d, J = 8.6, H-5), 8.45 (d, J = 1.7, H-8), 8.89 (s, H-2), 14.16 (b, NH), 14.67 (b, COOH).

General Procedure for the Synthesis of Ethyl 4-[3-(2,4-dichlorobenzylcarbamoyl)-1-ethyl-6-fluoro-4-*oxo*-1,4-dihydroquinoline-7-yl)]piperazine-1-carboxylate (22) and Ethyl 4-[1-cyclopropyl-3-(2,4-dichlorobenzylcarbamoyl)-6-fluoro-4-*oxo*-1,4-dihydroquinoline-7-yl)]piperazine-1-carboxylate (23). Norfloxacin and ciprofloxacin (1 equiv, 3 mmol) and 6 equiv (18 mmol) of NEt_3 were dissolved in abs DMF (40 mL). Ethyl chloroformate (5 equiv, 15 mmol) was added under stirring at 0 °C for 1 h and subsequently stirred at room temperature for 4 h. Then 50 mL of distilled H_2O were added, the solution was extracted with ethyl acetate (4 × 50 mL), and the combined organic layers were dried over anhydrous Na_2SO_4. The solvent was removed in vacuo, and the resulting residue dissolved in a mixture of 15 mL of DMF and 3 mL of NEt_3. Ethyl chloroformate (5 equiv, 15 mmol) of was added under stirring at 0 °C for 1 h, and 3 equiv (9 mmol) of 2,4-dichlorobenzylamine was added and stirred at room temperature for 3 d. After 50 mL of distilled H_2O were added, the solution was extracted with ethyl acetate (3 × 70 mL) and the combined organic layers dried over anhydrous Na_2SO_4. The solvent was removed in vacuo and the residue purified by column chromatography on silica gel (eluent: ethyl acetate/ethanol 30:1) to give **22** and **23**, respectively. **22**: yield 10%; mp 237−239 °C. IR [cm^{-1}]: 827, 1119, 1238, 1529, 1664, 1720, 2879, 2989, 3103, 3267. ^{1}H NMR (DMSO-d_6, δ [ppm], J [Hz]): 1.29 (t, J = 7.2, CH_3), 1.54 (t, J = 7.0, CH_3), 3.24−3.23 (m, 4 × piperazinyl-H), 3.72−3.69 (m, 4 × piperazinyl-H), 4.19 (q, J = 7.2, CH_2), 4.26 (q, J = 7.0, H_2), 4.70 (d, J = 5.6, CH_2), 6.80 (d, $J_{F,H}$ = 6.8, H-8), 7.19 (dd, J = 8.5, J = 2.0, benzyl-H), 7.38 (d, J = 2.0, benzyl-H), 7.39 (d, J = 8.5, benzyl-H), 8.09 (d, $J_{F,H}$ = 13.1, H-5), 8.71 (s, H-2), 10.50 (t, J = 5.6, NH). ^{13}C NMR (DMSO-d_6, δ [ppm], J [Hz]): 14.9 (CH_3), 15.1 (CH_3), 41.1 (CH_2), 44.0 (2 × piperazinyl-C), 50.0 (CH_2), 50.4 (2 × piperazinyl-C), 62.2 (CH_2), 104.4 (d, $J_{C,F}$ = 2.9, C-8), 111.8 (C-3), 113.7 (d, $J_{C,F}$ = 22.7, C-5), 123.4 (d, $J_{C,F}$ = 2.9, C-4a), 127.6 (benzyl-C), 129.7 (benzyl-C), 130.8 (benzyl-C), 133.9 (benzyl-C), 134.6 (benzyl-C), 135.5 (benzyl-C), 136.9 (C-8a), 145.5 (d, $J_{C,F}$ = 11.0, C-7), 147.2 (C-2), 153.7 (d, $J_{C,F}$ = 248.8, C-6), 155.9 ($NHRCO_2R$), 165.7 (CONH), 175.8 (d, $J_{C,F}$ = 2.2, C-4). **23**: yield 14%; mp 220−222 °C. IR [cm^{-1}]: 1119, 1240, 1562, 1608, 1626, 1666, 1716, 2945, 2981, 3095. ^{1}H NMR (DMSO-d_6, δ [ppm], J [Hz]): 1.16 (b, 2 × cyclopropyl-H), 1.29 (t, J = 7.1, CH_3), 1.33−1.32 (m, 2 × cyclopropyl-H), 3.26−3.24 (m, 4 × piperazinyl-H), 3.45 (b, cyclopropyl-H), 3.72−3.70 (m, 2 × piperazinyl-H), 4.19 (q, J = 7.1, H_2), 4.68 (d, J = 6.0, CH_2), 7.18 (dd, J = 8.3, J = 2.0, benzyl-H), 7.32 (d, $J_{F,H}$ = 7.1, H-8), 7.37 (d, J = 2.0, benzyl-H), 7.38 (d, J = 8.3, benzyl-H), 8.04 (d, $J_{F,H}$ = 13.1, H-5), 8.81 (s, H-2), 10.46 (t, J = 6.0, NH). ^{13}C NMR (DMSO-d_6, δ [ppm], J [Hz]): 8.32 (2 × cyclopropyl-C), 14.8 (CH_3), 34.9 (cyclopropyl-C), 40.7 (CH_2), 43.6 (2 × piperazinyl-C), 50.0 (2 × piperazinyl-C), 61.8 (CH_2), 105.1 (d, $J_{C,F}$ = 2.9, C-8), 111.3 (C-3), 113.0 (d, $J_{C,F}$ = 22.7, C-5), 122.3 (d, $J_{C,F}$ = 3.7, C-4a), 127.3 (benzyl-C), 129.3 (benzyl-C), 130.5 (benzyl-C), 133.6 (benzyl-C), 134.3 (benzyl-C), 135.1 (benzyl-C), 138.6 (C-8a), 144.9 (d, $J_{C,F}$ = 11.7, C-7), 147.1 (C-2), 153.6 (d, $J_{C,F}$ = 249.6, C-6), 155.5 ($NHRCO_2R$), 165.3 (CONH), 175.6 (C-4).

Cells and Viruses. Vero (African green monkey, ATCC CRL 6318), Vero E6, and MDCK (Madin−Darby canine kidney) cells were grown in Eagle's minimal essential medium (MEM, Gibco) supplemented with 10% fetal calf serum (FCS, Biochrom), 100 U/mL penicillin, and 100 μg/mL streptomycin. The NiV strain used in this work was isolated from human brain tissue (kindly provided by Jane Cardosa, Institute of Health and Community Medicine, University Malaysia Sarawak, Malaysia) and propagated in Vero E6 cells. Stock virus was harvested when the cytopathic effect was maximal. For infection, target cells were incubated for 1 h at 37 °C with NiV and then medium containing 2% FCS was added and the cells were further incubated for 24 h.

NiV G and F Expression Plasmids and Transfection. To obtain the two expression plasmids pczCFG5-NiVG and pczCFG5-NiVFtag, DNA fragments comprising the NiV open reading frames for G and F were cloned into a derivative of the replication-deficient murine leukemia virus vector pczCFG5 expressing in addition a zeocin resistance gene fused to the enhanced green fluorescent protein (EGFP) gene.[43,44] For transient expression, cells were transfected using polyethylenimine (PEI 25 kDa; Polyscience). Briefly, a monolayer of 4×10^5 Vero cells per well of a six-well plate were washed with prewarmed medium, and the mixture of 2 μg DNA in 50 μL of serum-free medium and 3 μL of PEI (from 1 mg/mL stock in serum-free medium) in 50 μL of serum-free medium (incubated for 30 min at RT) was added to the 1 mL medium per well, and subsequently compounds were added to the wells. Syncytia were observed after 24 h incubation at 37 °C.

Cell Vitality Assay. The tetrazolium salt 3-(4,5-dimethylthiazol-2-yl)-2,5-diphenyl-tetrazoliumbromide (MTT; Sigma) was incorporated in living cells and converted into a violet formazan product by mitochondrial dehydrogenases. Only living, vital cells and cells in the very early phase of apoptosis can transform MTT to crystals. Vero cells (1×10^5) in a six-well plate were preincubated for 16 h with chemical compounds. Medium was removed and cells incubated for 2 h with 1 mL/well fresh medium (MEM 5% FCS). After removal of the medium, cells were incubated for 2 h at 37 °C with 750 μL of MTT solution per well. Subsequently, the solution was removed and cells incubated for 45 min at RT with 750 μL of extraction solution. Then 12 × 50 μL aliquots were transferred into a 96-well plate and evaluated using an ELISA reader measuring the absorbance at 570 nm. Results (mean values) were presented as % vitality in relation to untreated healthy cells.

Molecular Modeling. The protein structure of the NiV postfusion coiled coil trimer was downloaded from the PDB (1WP7[20]). The structure was preprocessed using the Schrodinger Protein Preparation Guide:[45] hydrogens were added to the

structure, H-bonds within the protein were optimized, and the protein was minimized to an rmsd of 0.3 Å. The two-dimensional structures of the compounds to be docked were sketched in Marvin Sketch[46] and converted to three-dimensional structures using Molecular Networks' CORINA.[47] Possible chiral and tautomeric states were enumerated using Schrodinger LigPrep.[48] The ligands were then docked into the previously defined binding pocket using Schrodinger Glide XP with default settings.[49]

Acknowledgment. Thanks are due to Sabine Kendl and Doreen Luttge for technical assistance and the Deutsche Forschungsgemeinschaft (SFB 630) for financial support.

Supporting Information Available: Experimental procedures, analytical and spectral data of all synthesized compounds. This material is available free of charge via the Internet at http://pubs.acs.org.

References

(1) Murray, K.; Selleck, P.; Hooper, P.; Hyatt, A.; Gould, A.; Gleeson, L.; Westbury, H.; Hiley, L.; Selvey, L.; Rodwell, B.; Ketterer, P. A morbillivirus that caused fatal disease in horses and humans. *Science* **1995**, *268*, 94–97.
(2) O'Sullivan, J. D.; Allworth, A. M.; Paterson, D. L.; Snow, T. M.; Boots, R.; Gleeson, L. J.; Gould, A. R.; Hyatt, A. D.; Bradfield, J. Fatal encephalitis due to novel paramyxovirus transmitted from horses. *Lancet* **1997**, *349*, 93–95.
(3) Wang, L.; Harcourt, B. H.; Yu, M.; Tamin, A.; Rota, P. A.; Bellini, W. J.; Eaton, B. T. Molecular biology of Hendra and Nipah viruses. *Microbes Infect*. **2001**, *3*, 279–287.
(4) Chua, K. B.; Koh, C. L.; Hooi, P. S.; Wee, K. F.; Khong, J. H.; Chua, B. H.; Chan, Y. P.; Lim, M. E.; Lam, S. K. Isolation of Nipah virus from Malaysian Island flying foxes. *Microbes Infect*. **2002**, *4*, 145–151.
(5) Halpin, K.; Young, P. L.; Field, H. E.; Mackenzie, J. S. Isolation of Hendra virus from pteropid bats: a natural reservoir of Hendra virus. *J. Gen. Virol*. **2000**, *81*, 1927–1932.
(6) Chua, K. B. Nipah virus outbreak in Malaysia. *J. Clin. Virol*. **2003**, *26*, 265–275.
(7) Butler, D. Fatal fruit bat virus sparks epidemics in southern Asia. *Nature* **2004**, *429*, 7.
(8) Chadha, M. S.; Comer, J. A.; Lowe, L.; Rota, P. A.; Rollin, P. E.; Bellini, W. J.; Ksiazek, T. G.; Mishra, A. Nipah virus-associated encephalitis outbreak, Siliguri, India. *Emerging Infect. Dis*. **2006**, *12*, 235–240.
(9) Enserink, M. Emerging infectious diseases. Nipah virus (or a cousin) strikes again. *Science* **2004**, *303*, 1121.
(10) Hsu, V. P.; Hossain, M. J.; Parashar, U. D.; Ali, M. M.; Ksiazek, T. G.; Kuzmin, I.; Niezgoda, M.; Rupprecht, C.; Bresee, J.; Breiman, R. F. Nipah virus encephalitis reemergence, Bangladesh. *Emerging Infect. Dis*. **2004**, *10*, 2082–2087.
(11) Wong, K. T.; Shieh, W. J.; Kumar, S.; Norain, K.; Abdullah, W.; Guarner, J.; Goldsmith, C. S.; Chua, K. B.; Lam, S. K.; Tan, C. T.; Goh, K. J.; Chong, H. T.; Jusoh, R.; Rollin, P. E.; Ksiazek, T. G.; Zaki, S. R. Nipah virus infection: pathology and pathogenesis of an emerging paramyxoviral zoonosis. *Am. J. Pathol*. **2002**, *161*, 2153–2167.
(12) Negrete, O. A.; Levroney, E. L.; Aguilar, H. C.; Bertolotti-Ciarlet, A.; Nazarian, R.; Tajyar, S.; Lee, B. EphrinB2 is the entry receptor for Nipah virus, an emergent deadly paramyxovirus. *Nature* **2005**, *436*, 401–405.
(13) Negrete, O. A.; Wolf, M. C.; Aguilar, H. C.; Enterlein, S.; Wang, W.; Muhlberger, E.; Su, S. V.; Bertolotti-Ciarlet, A.; Flick, R.; Lee, B. Two key residues in ephrinB3 are critical for its use as an alternative receptor for Nipah virus. *PLoS Pathog*. **2006**, *2*, e7.
(14) Diederich, S.; Moll, M.; Klenk, H. D.; Maisner, A. The nipah virus fusion protein is cleaved within the endosomal compartment. *J. Biol. Chem*. **2005**, *280*, 29899–29903.
(15) Diederich, S.; Thiel, L.; Maisner, A. Role of endocytosis and cathepsin-mediated activation in Nipah virus entry. *Virology* **2008**, *375*, 391–400.
(16) Vogt, C.; Eickmann, M.; Diederich, S.; Moll, M.; Maisner, A. Endocytosis of the Nipah virus glycoproteins. *J. Virol*. **2005**, *79*, 3865–3872.
(17) Bentz, J. Membrane fusion mediated by coiled coils: a hypothesis. *Biophys. J*. **2000**, *78*, 886–900.
(18) Lamb, R. A. Paramyxovirus fusion: a hypothesis for changes. *Virology* **1993**, *197*, 1–11.
(19) Weissenhorn, W.; Dessen, A.; Calder, L. J.; Harrison, S. C.; Skehel, J. J.; Wiley, D. C. Structural basis for membrane fusion by enveloped viruses. *Mol. Membr. Biol*. **1999**, *16*, 3–9.
(20) Lou, Z.; Xu, Y.; Xiang, K.; Su, N.; Qin, L.; Li, X.; Gao, G. F.; Bartlam, M.; Rao, Z. Crystal structures of Nipah and Hendra virus fusion core proteins. *FEBS J*. **2006**, *273*, 4538–4547.
(21) Xu, Y.; Lou, Z.; Liu, Y.; Cole, D. K.; Su, N.; Qin, L.; Li, X.; Bai, Z.; Rao, Z.; Gao, G. F. Crystallization and preliminary crystallographic analysis of the fusion core from two new zoonotic paramyxoviruses, Nipah virus, and Hendra virus. *Acta Crystallogr., Sect. D: Biol. Crystallogr*. **2004**, *60*, 1161–1164.
(22) Xu, K.; Rajashankar, K. R.; Chan, Y. P.; Himanen, J. P.; Broder, C. C.; Nikolov, D. B. Host cell recognition by the henipaviruses: crystal structures of the Nipah G attachment glycoprotein and its complex with ephrin-B3. *Proc. Natl. Acad. Sci. U.S.A*. **2008**, *105*, 9953–9958.
(23) Bowden, T. A.; Crispin, M.; Harvey, D. J.; Aricescu, A. R.; Grimes, J. M.; Jones, E. Y.; Stuart, D. I. Crystal structure and carbohydrate analysis of Nipah virus attachment glycoprotein: a template for antiviral and vaccine design. *J. Virol*. **2008**, *82*, 11628–11636.
(24) Plemper, R. K.; Erlandson, K. J.; Lakdawala, A. S.; Sun, A.; Prussia, A.; Boonsombat, J.; Aki-Sener, E.; Yalcin, I.; Yildiz, I.; Temiz-Arpaci, O.; Tekiner, B.; Liotta, D. C.; Snyder, J. P.; Compans, R. W. A target site for template-based design of measles virus entry inhibitors. *Proc. Natl. Acad. Sci. U.S.A*. **2004**, *101*, 5628–5633.
(25) Plemper, R. K.; Doyle, J.; Sun, A.; Prussia, A.; Cheng, L. T.; Rota, P. A.; Liotta, D. C.; Snyder, J. P.; Compans, R. W. Design of a small-molecule entry inhibitor with activity against primary measles virus strains. *Antimicrob. Agents Chemother*. **2005**, *49*, 3755–3761.
(26) Sun, A.; Prussia, A.; Zhan, W.; Murray, E. E.; Doyle, J.; Cheng, L. T.; Yoon, J. J.; Radchenko, E. V.; Palyulin, V. A.; Compans, R. W.; Liotta, D. C.; Plemper, R. K.; Snyder, J. P. Nonpeptide inhibitors of measles virus entry. *J. Med. Chem*. **2006**, *49*, 5080–5092.
(27) Gould, R. G.; Jacobs, W. A. The synthesis of certain substituted quinolines and 5,6-benzoquinolines. *J. Am. Chem. Soc*. **1939**, *61*, 2890–2895.
(28) Leyva, E.; Monreal, E.; Hernandez, A. Synthesis of fluoro-4-hydroxyquinolone-3-carboxylic acids by the Gould−Jacobs reaction. *J. Fluorine Chem*. **1999**, *94*, 7–10.
(29) Heaney, H.; Ley, S. V. *N*-Alkylation of indole and pyrroles in dimethyl sulphoxide. *J. Chem. Soc., Perkin Trans*. **1973**, *1*, 499-500.
(30) Albaugh, P.; Currie, K.; Rosewater, D.; Cai, G. Substituted 4-*oxo*-quinoline-3-carboxamides: GABA brain receptor ligands. Patent WO/2000/068202, PCT/US2000/012096, 2000.
(31) Schohe-Loop, R.; Zimmermann, H.; Henninger, K.; Paulsen, D.; Rolle, T.; Lang, D.; Thede, K.; Furstner, C.; Bruckner, D.; Kobberling, J.; Bauser, M. Substituted Quinolones. Patent WO/2006/008046, PCT/EP2005/007601, 2006.
(32) Snyder, H. R.; Freier, H. E.; Kovacic, P.; Van Heyningen, E. M. Synthesis of 4-hydroxyquinolines. VIII. Some halogen-containing 4-aminoquinoline derivatives. *J. Am. Chem. Soc*. **1947**, *69*, 371–374.
(33) Koga, H.; Itoh, A.; Murayama, S.; Suzue, S.; Irikura, T. Structure−activity relationships of antibacterial 6,7- and 7,8-disubstituted 1-alkyl-1,4-dihydro-4-oxoquinoline-3-carboxylic acids. *J. Med. Chem*. **1980**, *23*, 1358–1363.
(34) Shah, K. J.; Coats, E. A. Design, synthesis, and correlation analysis of 7-substituted 4-hydroxyquinoline-3-carboxylic acids as inhibitors of cellular respiration. *J. Med. Chem*. **1977**, *20*, 1001–1006.
(35) Podányi, B.; Keresztúri, G.; Vasvári-Debreczy, L.; Chinoin, I. H.; Tóth, G. An NMR study of halogenated 1,4-dihydro-1-ethyl-4-oxoquinoline-3-carboxylates. *Magn. Reson. Chem*. **1996**, *11*, 972–978.
(36) Ridgway, H. M.; Waters, D. M.; Peel, M. E.; Ellis, Pennant, G. Tetrazolyloxodihydroquinolinecarboxamides. Patent DE/2407744/19740829, 1974.
(37) MDL Drug Data Report (MDDR); Symyx Technologies, Inc.: Santa Clara, CA: 2005.
(38) Grant, J. A.; Gallardo, M. A.; Pickup, B. A fast method of molecular shape comparison. A simple application of a Gaussian description of molecular shape. *J. Comput. Chem*. **1996**, *17*, 1653–1666.
(39) Mitscher, L. A. Bacterial topoisomerase inhibitors: quinolone and pyridone antibacterial agents. *Chem. Rev*. **2005**, *105*, 559–592.

(40) Bradbury, B. J.; Pucci, M. J. Recent advances in bacterial topoisomerase inhibitors. *Curr. Opin. Pharmacol.* **2008**, *8*, 574–581.
(41) Goebel, T.; Ulmer, D.; Projahn, H.; Kloeckner, J.; Heller, E.; Glaser, M.; Ponte-Sucre, A.; Specht, S.; Sarite, S. R.; Hoerauf, A.; Kaiser, A.; Hauber, I.; Hauber, J.; Holzgrabe, U. In search of novel agents for therapy of tropical diseases and human immunodeficiency virus. *J. Med. Chem.* **2008**, *51*, 238–250.
(42) Cianci, C.; Meanwell, N.; Krystal, M. Antiviral activity and molecular mechanism of an orally active respiratory syncytial virus fusion inhibitor. *J. Antimicrob. Chemother.* **2005**, *55*, 289–292.
(43) Lindemann, D.; Pietschmann, T.; Picard-Maureau, M.; Berg, A.; Heinkelein, M.; Thurow, J.; Knaus, P.; Zentgraf, H.; Rethwilm, A. A particle-associated glycoprotein signal peptide essential for virus maturation and infectivity. *J. Virol.* **2001**, *75*, 5762–5771.
(44) Moll, M.; Diederich, S.; Klenk, H. D.; Czub, M.; Maisner, A. Ubiquitous activation of the Nipah virus fusion protein does not require a basic amino acid at the cleavage site. *J. Virol.* **2004**, *78*, 9705–9712.
(45) Protein Preparation Guide; Schrodinger, LLC: New York, 2007.
(46) Marvin Sketch; ChemAxon Kft; Budapest, 2008.
(47) 3D Structure Generator CORINA: Generation of High-Quality Three-Dimensional Molecular Models; Molecular Networks GmbH Computerchemie: Erlangen, Germany, 2006.
(48) LigPrep; Schrodinger, LLC: New York, 2007.
(49) Glide; Schrodinger, LLC: New York, 2007.